Theory and Design of OTA-C Oscillators with Native Amplitude Limiting

Kofi M. Odame, *Student Member, IEEE*, and Paul Hasler, *Senior Member, IEEE*

***Abstract*—An analog sinusoidal oscillator usually involves some form of amplitude-limiting mechanism. We examine operational-transconductance-amplifier (OTA) nonlinearity as a choice for amplitude limiting and develop a general theory for its use in OTA–capacitor (OTA-C) oscillators. We facilitate our theoretical discussion with an illustrative design example that we fabricated and tested.**

***Index Terms*—Nonlinear oscillators.**

I. Oscillator Design Approaches

THE SINUSOIDAL oscillator is a basic analog-circuit component in communication and instrumentation systems. High-quality oscillators usually involve inductor–capacitor networks and are used in RF systems. However, the inductance values required for low- and moderate-frequency oscillators cannot practically be realized in integrated circuits. Ring oscillators provide much better economy in terms of size, but they are limited to such uses as clock generation due to their high harmonic content. Operational transconductance amplifier–capacitor (OTA-C) oscillators, on the other hand, operate at low to moderate frequencies with fairly high spectral purity and are compact enough for integration. An OTA-C oscillator is typically designed as an unstable second-order system that is regulated by some nonlinear amplitude-limiting circuitry. Buonomo *et al.*[1] identified a set of conditions on the nonlinearity for the system to exhibit oscillation. The most common implementations of an amplitude limiter are a piecewise-linear resistor and an automatic gain control circuit [1]–[4]. A third possibility is to use the inherent nonlinear behavior of an OTA as an amplitude limiter.

The success of using OTA nonlinearity, as reported in the literature, has been mixed. This approach is considered in [3], but the results are only poorly controlled distorted oscillations. The approach is also mentioned in [2] but is characterized as yielding only unpredictable oscillations. On the other hand, the results in [5], [6], and [7] show success in designing sinusoidal oscillators based on OTA nonlinearity. However, none of these papers, nor, to our knowledge, any other sources in the literature, provide a systematic and analytical presentation of how exactly to exploit OTA nonlinearity in a general second-order oscillator structure. This is a relevant lack, as an oscillator that properly exploits OTA nonlinearity can easily confer power and area savings, since no external amplitude-limiting scheme is required. For instance, a slight redesign of the oscillator in [2] could have used one of the existing OTAs as an amplitude limiter, precluding the need for the extra piecewise-linear (PWL) circuit that its authors describe.

Manuscript received April 11, 2006; revised July 18, 2007. First published May 20, 2008; current version published February 4, 2009. This paper was recommended by Associate Editor G. Cauwenberghs.

The authors are with the School of Electrical and Computer Engineering, Georgia Institute of Technology, Atlanta, GA 30332-0760 USA (e-mail: odame@ece.gatech.edu).

Digital Object Identifier 10.1109/TCSI.2008.925819

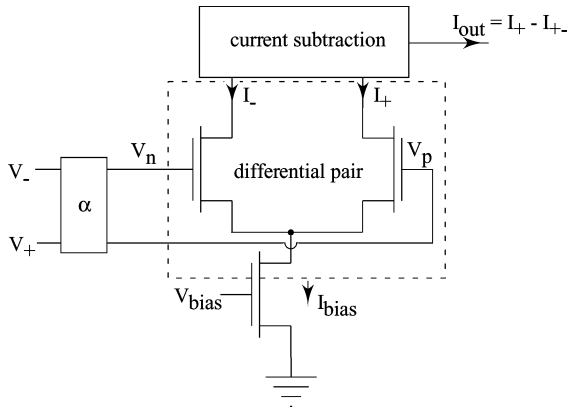

Fig. 1. OTA converts a differential voltage input into an output current. A differential pair of transistors is at the heart of the voltage–current conversion. An attenuating stage may exist between the voltage input and the differential pair. A current-subtraction network combines the drain currents of the differential-pair transistors into a single output.

This paper provides a rigorous generalized method for exploiting OTA nonlinearity in oscillator design and is organized as follows. Section II introduces the OTA and its transfer-function equations. Section III presents intuitive motivation for using OTA nonlinearity for oscillator design. Section IV-A presents a generalized model for a second-order OTA-C circuit. In Section IV-B, the results developed in the preceding sections are used to formulate an oscillator synthesis methodology, using OTA nonlinearity for amplitude limiting. Section V analyzes the oscillator that would result from our synthesis methodology. Section VI addresses certain implementation issues that arise due to our particular synthesis procedure. Section VII illustrates our technique with a simple OTA-C second-order section (SOS), which we fabricated in a 0.5-μm CMOS process. This section compares experimental measurements of our oscillator with the theoretical predictions. Finally, Sections VIII and IX are the discussion and conclusion of the paper, respectively.

II. OTA Basics

A. Output Current

Fig. 1 shows a block-diagram representation of an OTA. The differential input, $V_{\rm in} = V_+ - V_-$, is applied to an attenuating stage. The output of the attenuating stage is fed into the gate

voltages of a differential pair, which is normally in saturation. A current-subtraction network generates the difference of the differential pair's drain currents, $I_{\text{out}} = I_+ - I_-$. The OTA thus provides a *transconductance* function from V_{in} to I_{out}.

If the differential pair is biased in the subthreshold region, then the voltage–current function is [8]

$$I_{\text{out}} = I_{\text{bias}} \tanh\left(\frac{\kappa\alpha V_{\text{in}}}{2U_T}\right) \tag{1}$$

where κ is the body-effect coefficient and U_T is the thermal voltage [9]. In addition, I_{bias} is a tunable bias current, and α is the gain of the attenuating stage. If the differential pair is biased above threshold, then, using the transistor model of [9], the OTA's voltage–current function can be found to be

$$I_{\text{out}} = \alpha\sqrt{\kappa\beta I_{\text{bias}}}V_{\text{in}}\sqrt{1 - \frac{\kappa\beta\alpha^2 V_{\text{in}}^2}{4I_{\text{bias}}}} \tag{2}$$

where β is a physical constant that is related to the differential pair's geometry and to doping concentrations. Again, I_{bias} is a tunable bias current, and α is the gain of the attenuating stage.

If we define a characteristic voltage V_c as

$$V_c = \begin{cases} \frac{2U_T}{\kappa}, & \text{subthreshold} \\ \sqrt{\frac{I_{\text{bias}}}{\kappa\beta}}, & \text{above threshold} \end{cases} \tag{3}$$

and the transconductance gain as $G_m = \alpha I_{\text{bias}}/V_c$, then we can write (1) and (2) as

$$I_{\text{out}} = \frac{G_m V_c}{\alpha} \cdot H\left(\frac{\alpha V_{\text{in}}}{V_c}\right) \tag{4}$$

where $H(\cdot)$ is a sigmoidal function that depends on the region of operation. In general, it would also depend on the specific OTA topology. Equation (4) is generic enough to describe any OTA with a saturating transfer curve, regardless of specific topology or of region of operation. V_c can be chosen to be any appropriate voltage. In this paper, we choose V_c such that the coefficient of the Taylor series linear term of $H(\cdot)$ is normalized to one.

B. Linear Versus Nonlinear OTAs

In this paper, we will regard some OTAs as linear elements and others as nonlinear ones. This section clarifies what the distinction is. Consider the Maclaurin series expansion of the OTA output current I_{out}

$$I_{\text{out}} = \frac{G_m V_c}{\alpha} \underbrace{\left(\frac{\alpha V_{\text{in}}}{V_c} + \sum_{i=2}^{\infty} \frac{H^{(i)}(0)}{i!}\left(\frac{\alpha V_{\text{in}}}{V_c}\right)^i\right)}_{H(z)}. \tag{5}$$

The small-signal transconductance gain is the linear-term coefficient, denoted by G_m in the earlier equations. An OTA is considered linear if, for the region of operation of V_{in}, its output current can be reasonably modeled—as appropriate to the application in question—as $I_{\text{out}} = G_m V_{\text{in}}$. For the nonlinear terms to be negligible, their coefficients must be sufficiently small. In this paper, we will make an OTA linear by making α small enough.

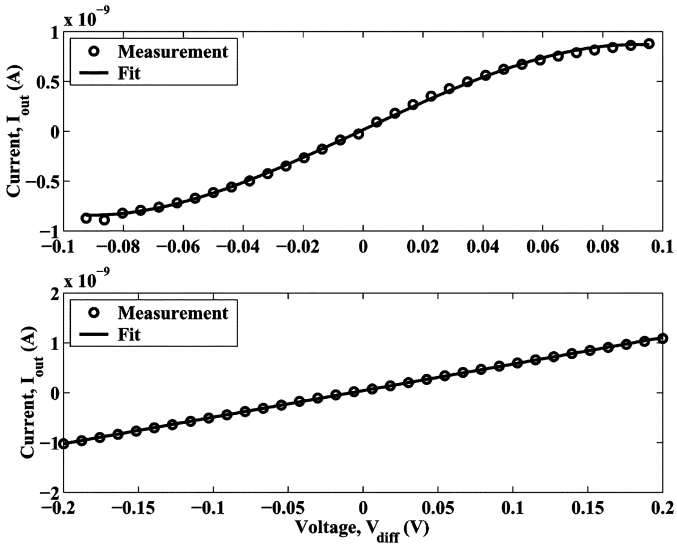

Fig. 2. Upper panel shows experimental measurements from a nonlinear OTA. In the lower panel, the nonlinear terms are suppressed enough for a straight line to be an accurate approximation over a 400-mV range.

For larger values of α, the nonlinear terms in (5) become comparatively significant to the linear term, and the OTA is considered nonlinear. In this paper, we will assume that a nonlinear OTA has a value of $\alpha = 1$. Fig. 2 shows a comparison of the output current of a nonlinear OTA ($\alpha = 1$) to that of a linear one ($\alpha = 0.1$).

III. Motivation for Using OTA as an Amplitude Limiter

Oscillator circuits are typically based on implementing Liénard's equation

$$\ddot{z} + f(z)\dot{z} + \gamma(z) = 0. \tag{6}$$

If $f(z)$ and $\gamma(z)$ satisfy the Liénard's theorem conditions, then the circuit will have a unique stable oscillation [11]. Notice that the theorem does not guarantee an oscillation that is sinusoidal, or even near-sinusoidal. For (6) to be relevant to a discussion of sinusoidal oscillators, where phase noise is low, $\gamma(z)$ must be linear. The damping term, however, is nonlinear. In practice, it can be obtained by taking the derivative of a nonlinear negative resistor, whose transfer function is shown in Fig. 3(a).

It is fairly straightforward to synthesize the nonlinear resistor with a pair of OTAs, one linear and the other nonlinear. Consider the OTAs shown in Fig. 4. Assuming that the amplifier that is in the positive-feedback configuration has an attenuation factor of one and that the one in the negative-feedback configuration has an attenuation factor of α, we can write the total output current as

$$I_{\text{out}} = \frac{G_{mL} V_{cL}}{\alpha} \cdot H\left(\frac{\alpha V_z}{V_{cL}}\right) - G_m V_c \cdot H\left(\frac{V_z}{V_c}\right). \tag{7}$$

If $\alpha \ll 1$, then the negative-feedback OTA is effectively linear, in which case I_{out} is approximately

$$I_{\text{out}} \approx G_{mL} V_z - G_m V_c \cdot H\left(\frac{V_z}{V_c}\right). \tag{8}$$

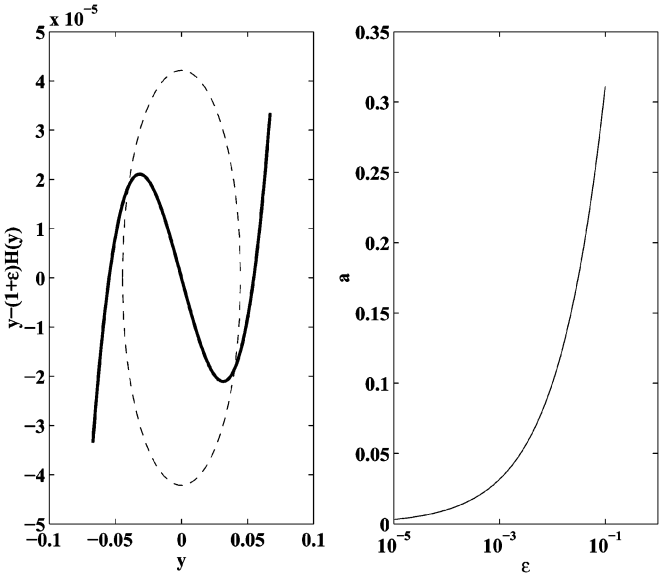

Fig. 3. (a) Region of oscillation and (b) dependence on ϵ.

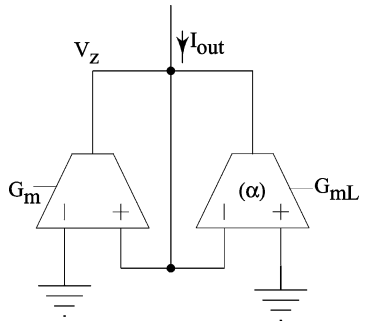

Fig. 4. OTA implementation of nonlinear resistor. The linear range of the negative-feedback OTA is much greater than that of the positive-feedback OTA. The bias current of the nonlinear OTA is slightly larger than I_b.

Now, imagine that the transconductance gain of the nonlinear OTA is slightly larger than that of the linear one. That is

$$G_m = (1+\rho)G_{mL} \tag{9}$$

where ρ is a small positive number. Then, the general shape of (8) is of that shown in Fig. 3(a). The attraction of implementing the nonlinear resistor as such is that it merely depends on manipulation of OTA linear ranges and bias currents, rather than on the addition and design of other types of circuit elements.

If we implement the nonlinear resistor as described, then, after nondimensionalization of (8), (6) becomes

$$\ddot{z} + \underbrace{\frac{\mathrm{d}}{\mathrm{d}z}\left(z-(1+\rho)H(z)\right)}_{f(z)}\dot{z} + z = 0 \tag{10}$$

where we have set $\gamma(z) = z$.

We can glean some intuition about the system's oscillatory behavior by studying Fig. 3(a). Close to the origin, the slope (i.e., $f(z)$) is negative, which implies negative damping. Therefore, energy is pumped into the system of (6) when it is close to the origin, ensuring a self-starting condition. Farther from the origin, damping is positive, which limits the amplitude of the signal.

Once steady-state oscillation is achieved, the movement of the system's signal is confined to the dashed region of Fig. 3(a). The size of this region can be found by calculating the location of the extrema of $z-(1+\rho)H(z)$. Fig. 3(b) shows a plot of the region size versus ρ. Note that the oscillation region size is also dependent on $H(z)$.

Within the region of oscillation, $f(z)$ may be approximated by the following even-order function:

$$f(z) \approx -\rho\left(\frac{1-z^2}{m_\rho^2}\right) \tag{11}$$

where m_ρ is a function of ρ such that $f(m_\rho) = 0$. This approximation is derived from noting that $H(z)$ is dominantly cubic and then fitting a quadratic function to pass through the point $(0, f(0))$ and the roots of $f(z)$. Equation (10) is now approximately

$$\ddot{z} - \rho\left(\frac{1-z^2}{m_\rho^2}\right)\dot{z} + z = 0, \qquad \rho > 0. \tag{12}$$

We identify a perturbation parameter, $\epsilon = \rho$, and define $y = z/m_\rho$ to write

$$\ddot{y} - \epsilon(1-y^2)\dot{y} + y = 0, \qquad \epsilon > 0. \tag{13}$$

From Liénard's theorem, (13) exhibits a stable unique oscillation. Furthermore, since it is just a perturbation of a linear resonator, we can expect very nearly sinusoidal oscillations for small enough ϵ. The behavior of this oscillator can be analyzed using multitimescale perturbation or via the method of averaging [14]. Note that Liénard's theorem is valid only if the nonlinearity is continuously differentiable. Even though most physical circuits have continuously differentiable transfer functions, there exists another analysis method, describing functions [3], that can handle the case of functions with discontinuous derivatives (i.e., piecewise linear functions).

IV. OTA-C Oscillator Synthesis

An OTA-C implementation of the Liénard equation will involve a SOS and some form of nonlinearity. The nonlinearity may be external to the SOS [1]–[4] or may be an inherent part of it [5], [6]. We espouse the latter approach and present in this paper a general method for synthesizing a sinusoidal oscillator this way.

A. Linear OTA-C SOSs

Fig. 5 shows a general OTA-C SOS [13]. It has two dominant poles, each of which is produced by a low-conductance/high-capacitance node. We can derive the governing dynamics of a SOS by applying Kirchhoff's current law (KCL) to each of its two nodes. The only way that current can flow onto a node is either through a capacitor or through an OTA. Assuming no floating nodes, there are at most three effective capacitors in an SOS: the two grounded capacitors at either node and the floating capacitor between both nodes. The inputs to any OTA can only be a linear combination of the node voltages. If all of the OTAs are operated linearly, then the sum of the OTA currents at a given

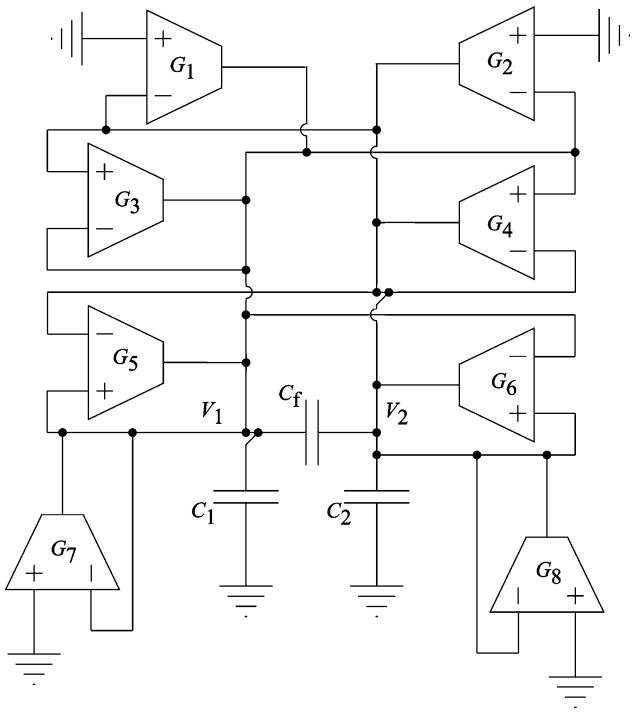

Fig. 5. Generic OTA-C SOS.

node is simply a linear combination of the node voltages. With all of the earlier constraints, any OTA-C SOS is fully described by [13]

$$\begin{bmatrix} C_1\dot{V}_1 \\ C_2\dot{V}_2 \end{bmatrix} = \begin{bmatrix} G_{11} & G_{12} \\ G_{21} & G_{22} \end{bmatrix} \begin{bmatrix} V_1 \\ V_2 \end{bmatrix} + C_f \begin{bmatrix} \dot{V}_2 - \dot{V}_1 \\ \dot{V}_1 - \dot{V}_2 \end{bmatrix} \tag{14}$$

where V_1 and V_2 are the node voltages. The quantities C_1, C_2, and C_f are the capacitances of the two grounded capacitors and of the floating capacitor, respectively. Finally, each G_{ij} is the effective OTA small-signal transconductance gain of V_j seen by the ith node. We make the following definitions:

$$\begin{aligned} \phi &= \frac{C_f}{C_1} \quad k = \frac{C_1}{C_2} \quad \tau = \frac{t \cdot G}{C_1} \\ x_1 &= \frac{V_1}{V_c} \quad x_2 = \frac{V_2}{V_c} \end{aligned} \tag{15}$$

where G is some representative transconductance gain; for example, $G = \max(G_{11-22})$. Once we introduce the nonlinear OTA, V_c will be defined in terms of the corresponding $H(y)$ nonlinearity. The quantities x_1 and x_2 are state variables that are scaled according to V_c. Applying the substitutions of (15), the dimensionless state-space form of (14) is

$$\begin{bmatrix} \dot{x}_1 \\ \dot{x}_2 \end{bmatrix} = \underbrace{\begin{bmatrix} a & b \\ c & d \end{bmatrix}}_{\boldsymbol{A}} \begin{bmatrix} x_1 \\ x_2 \end{bmatrix} + \phi \begin{bmatrix} \dot{x}_2 - \dot{x}_1 \\ k\dot{x}_1 - k\dot{x}_2 \end{bmatrix}. \tag{16}$$

The state variables x_1 and x_2 are differentiated with respect to the dimensionless independent variable τ. For most of this paper, we will assume that there are no floating capacitors in the SOS. That is, $\phi = C_f = 0$.

B. Conversion From a Linear SOS to an Oscillator

Our oscillator design is essentially a question of converting (10), (11), (12), (13), (14), (15), and (16). The one caveat is that this conversion to Liénard's equation be physically realizable, using a nonlinear OTA. Note that the OTA's only possible inputs are the state variables x_1, x_2. In addition, the OTA's output must be added directly to the dynamics of exactly one or the other state variable. Therefore, converting (16) to the Liénard equation can only involve adding a vector of the form

$$\begin{bmatrix} g_h \cdot H(px_1 + qx_2) \\ 0 \end{bmatrix} \quad \begin{bmatrix} 0 \\ g_h \cdot H(px_1 + qx_2) \end{bmatrix} \tag{17}$$

to the right-hand side of (16). Here, $H(\cdot)$ is the nonlinear OTA's sigmoidal function, and its argument is a weighted sum of x_1 and x_2. In addition, g_h is a dimensionless representation of the nonlinear OTA's small-signal transconductance gain. Successful oscillator design depends on choosing the appropriate values of p, q, and g_h.

1) Some Special Cases: We introduce our synthesis procedure with the simple SOS shown in Fig. 6(a), where the OTAs are linear and $G_{1,2}$ are their respective transconductance gains. By applying KCL, we derive the following state-space equation:

$$\begin{bmatrix} \dot{x}_1 \\ \dot{x}_2 \end{bmatrix} = \begin{bmatrix} 0 & b \\ c & d \end{bmatrix} \begin{bmatrix} x_1 \\ x_2 \end{bmatrix} \tag{18}$$

where $b \propto G_1$, $c \propto G_2$, and $d \propto G_2$. Notice that $\boldsymbol{A}$ is a lower skew-triangular matrix in this example. For $\boldsymbol{A}$ of this type, we convert (16) into the Liénard equation by simply adding $(\mu - d)H(x_2)$ to the x_2 dynamics. We have picked $p = 0, q = 1$, and $g_h = (\mu - d)$, where μ is to be determined. Adding $(\mu - d)H(x_2)$ to the x_2 dynamics of (18) yields

$$\begin{bmatrix} \dot{x}_1 \\ \dot{x}_2 \end{bmatrix} = \begin{bmatrix} bx_2 \\ cx_1 + dx_2 - (d - \mu)H(x_2) \end{bmatrix} \tag{19}$$

which, as a single differential equation, is

$$\ddot{x}_2 - (d - (d - \mu)H'(x_2))\,\dot{x}_2 - bcx_2 = 0. \tag{20}$$

As discussed earlier (see (12)), this can be approximated as

$$\ddot{x}_2 - \mu\left(\frac{1 - x_2^2}{m_\mu^2}\right)\dot{x}_2 - bcx_2 = 0 \tag{21}$$

where m_μ is a function of μ such that $H'(m_\mu) = d/(d - \mu)$.

If we define

$$\begin{aligned} y &= \frac{x_2}{m_\mu} \\ \mu &= \epsilon\sqrt{-bc} \end{aligned} \tag{22}$$

and rescale time as

$$T = \sqrt{-bc} \cdot \tau \tag{23}$$

then (20) becomes

$$\frac{\mathrm{d}^2 y}{\mathrm{d}T^2} - \epsilon\left(1 - y^2\right)\frac{\mathrm{d}y}{\mathrm{d}T} + y = 0 \tag{24}$$

the van der Pol equation. Note that, for the conversion to make sense, we must have $bc < 0$ and $d < 0$. From (19) and (22), we can infer the required placement of the nonlinear OTA. The

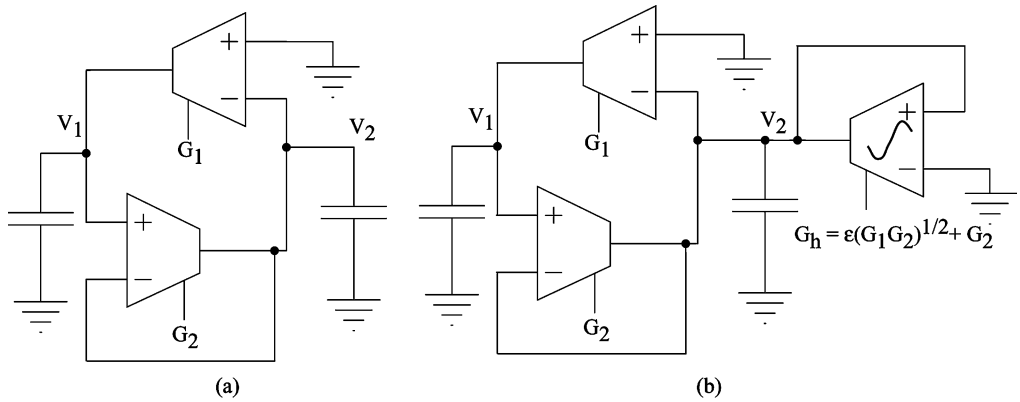

Fig. 6. Simple van der Pol derivation. (a) Initial SOS circuit, with all linear OTAs. (b) Nonlinear OTA converts SOS into the van der Pol oscillator.

positive input is x_2, the negative input is (a.c.) ground, and the output current is sourced onto node x_2. In addition, we must bias the nonlinear OTA such that its small-signal transconductance gain corresponds to $\epsilon\sqrt{-bc}-d$. Fig. 6(b) shows the augmented SOS circuit, now an oscillator.

If $\boldsymbol{A}$ is an upper skew-triangular matrix, then we can obtain an oscillator by a series of similar steps as earlier. We place a nonlinear OTA whose output and positive input are connected to node x_1. In addition, its negative output must be at ground, and it must be biased to have a small-signal gain corresponding to $\epsilon\sqrt{-bc}-a$. Again, we require $bc<0$ and also $a<0$.

2) General Case: When $\boldsymbol{A}$ is not skew triangular, it is a little trickier to convert (16) into the Liénard system. With the general form of (16), improper placement of the nonlinearity can cause unwanted distortion. The issue is that the dynamics of one state variable will couple into those of the other. Assuming $\phi=0$, we can reduce the interdependence of the states by changing the axes of the dynamical system.

Consider a new state vector, $\underline{v}=\begin{bmatrix}v_1 & v_2\end{bmatrix}^{\mathrm{T}}$, defined as

$$\begin{bmatrix}v_1\\ v_2\end{bmatrix}=\begin{bmatrix}x_1\\ cx_1+dx_2\end{bmatrix}. \tag{25}$$

Written in terms of $\underline{v}$, with $\phi=0$, (16) becomes

$$\begin{bmatrix}\dot{v}_1\\ \dot{v}_2\end{bmatrix}=\begin{bmatrix}a-\frac{bc}{d} & \frac{b}{d}\\ 0 & d\end{bmatrix}\begin{bmatrix}v_1\\ v_2\end{bmatrix}+\begin{bmatrix}0\\ c\dot{v}_1\end{bmatrix}. \tag{26}$$

We convert (26) into the Liénard equation by simply adding $g_h\cdot H(v_2)$ to the v_1 dynamics. Again, g_h refers to the small-signal gain of the nonlinear OTA. After adding the nonlinear OTA to (26), we arrive at the following second-order ODE

$$\ddot{v}_2-\left(a+d+cg_hH'(v_2)\right)\dot{v}_2+(ad-bc)\,v_2=0 \tag{27}$$

which is approximately

$$\ddot{v}_2-(a+d+cg_h)\left(\frac{1-v_2^2}{m_{gh}^2}\right)\dot{v}_2+(ad-bc)\,v_2=0 \tag{28}$$

where m_{gh} is such that $H'(m_{gh})=-(a+d)/(cg_h)$.

Next, we rescale time as $T=\sqrt{ad-bc}\cdot\tau$ and define

$$\epsilon=(a+d+cg_h)(ad-bc)^{-(1/2)} \tag{29}$$

$$y=\frac{v_2}{m_{gh}} \tag{30}$$

to get

$$\frac{\mathrm{d}^2y}{\mathrm{d}T^2}-\epsilon\left(1-y^2\right)\frac{\mathrm{d}y}{\mathrm{d}T}+y=0 \tag{31}$$

as desired. Note from (30) that we require

$$ad-bc>0 \tag{32}$$

$$a+d<0 \tag{33}$$

which are the same conditions for $\boldsymbol{A}$ to be Hurwitz. That is, the SOS must be stable[1]. These inequalities are consistent with those for when $\boldsymbol{A}$ is a skew-triangular matrix.

3) Summary: Any stable linear OTA-C SOS circuit can be converted into an oscillator via OTA nonlinearity. This is done by augmenting the linear SOS, (16), with a nonlinear OTA in the form of the first vector in (17), choosing

$$p=c\quad q=d \tag{34}$$

$$g_h=\frac{\left(\epsilon\sqrt{ad-bc}-(a+d)\right)}{c}. \tag{35}$$

Notice that we would have arrived at a very similar alternative solution had we defined $\underline{v}$ as

$$\begin{bmatrix}v_1\\ v_2\end{bmatrix}=\begin{bmatrix}ax_1+bx_2\\ x_2\end{bmatrix}. \tag{36}$$

V. Characteristics of the van der Pol Equation

OTA nonlinearity is an appealing choice for amplitude limiting in oscillators, because it is power- and area-efficient. When the nonlinearity results in the van der Pol oscillator, we enjoy the additional benefit of having implemented a well-known and studied dynamical system. The choices of design parameters for the oscillator can then be informed by analytical results from the field of perturbation theory.

[1]It is possible to convert an unstable SOS into an oscillator, using a procedure very similar to that which we have so far described. The main difference is that the nonlinearity involved would be expansive (as encountered, for instance, in a current feedback operational amplifier), rather than the usual OTA compressive function.

The van der Pol equation has no closed-form solution. However, for small enough ϵ, we can use first-order averaging to find the following approximate solution [14]:

$$y(T) = \frac{2\cos T}{\sqrt{1 - \mathrm{e}^{-\epsilon T}\left(1 + \frac{4}{y_0^2}\right)}} \tag{37}$$

where y_0 depends on initial conditions. Note that, as $T \to \infty$, the solution approaches a sinusoid of amplitude two. Furthermore, this approach is roughly at a rate of $\mathrm{e}^{-\epsilon T}$. The oscillator's start-up time is thus proportional to $1/\epsilon$.

Applying higher order perturbation analysis [14] reveals that, at steady state, the solution to (31) is

$$\begin{aligned} y(T) = & 2\cos(T) + \frac{3\epsilon}{4\sin(T)} - \frac{\epsilon^2}{8\cos(T)} \\ & \pm \frac{\epsilon}{4\sin(3T)} + \frac{3\epsilon^2}{16\cos(3T)} \\ & \pm \frac{5\epsilon^2}{96\cos(5T)} + O(\epsilon^3). \end{aligned} \tag{38}$$

We would ideally want an oscillator that has no higher order harmonics. The square-root of the ratio of harmonic power to fundamental frequency power is a measure of this nonideality and is referred to as total harmonic distortion (THD). From (38), we derive the following expression for THD

$$\begin{aligned} THD\% &= \frac{\epsilon}{8}\sqrt{\frac{1 + \frac{349\epsilon}{576}}{1 + \frac{\epsilon^2}{64} + \frac{\epsilon^4}{256}}} \cdot 100 \\ &\approx 12.5\epsilon + 3.8\epsilon^2. \end{aligned} \tag{39}$$

According to (29), ϵ depends on how much bigger g_h is than $|a + d|$. It is effectively a measure of the strength of the nonlinear OTA relative to the linear ones. That THD increases with ϵ matches our intuition that the oscillator's nonlinearity be "weak," or "soft."

VI. OTA-C Oscillator Analysis and Design Considerations

So far, our treatment has been mostly theoretical. In this section and Sections VII and VIII, we address the implications that our design framework has for a practical oscillator implementation.

A. Frequency of Oscillation

From (37), the system oscillates at a rate of one cycle per 2π units of T. Recalling $T = \tau\sqrt{ad - bc}$, and $\tau = tG/C_1$, this corresponds to an oscillation frequency of

$$w_o = G\sqrt{ad - bc}/C_1 \mathrm{rad}^{-1}. \tag{40}$$

The quantity G is some representative transconductance gain of the linear SOS of (14) (e.g., $G = \max(G_{11-22})$). If we maintain the relative gains of the amplifiers—i.e., a, b, c, and d are kept constant—then increasing G will cause a linear increase in the frequency of oscillation.

B. Amplitude of Oscillation

According to (37), the circuit oscillates at an amplitude of two units of the y quantity. In terms of the v_2 variable, the amplitude of oscillation is (see (30))

$$\mathrm{amp}(v_2) = 2m_{gh}. \tag{41}$$

From (25), v_2 is the derivative of x_2 with respect to τ. Using this fact and replacing x_2 and τ with their expressions in V_2 and t, respectively, we find the voltage amplitude of oscillation to be

$$\mathrm{amp}(V_2) = \frac{2m_{gh}V_c}{\sqrt{ad - bc}}. \tag{42}$$

Recall that m_{gh} is defined as

$$H'(m_{gh}) = -(a + d)/(cg_h). \tag{43}$$

Using the definition of ϵ, we can write

$$H'(m_{gh}) = \frac{-(a + d)}{\epsilon\sqrt{ad - bc} - (a + d)}. \tag{44}$$

The amplitude of oscillation is thus

$$\mathrm{amp}(V_2) = \frac{2V_c}{\sqrt{ad - bc}}(H')^{-1}\left(\frac{-(a + d)}{\epsilon\sqrt{ad - bc} - (a + d)}\right). \tag{45}$$

For small ϵ, the oscillation-amplitude equation can be simplified to

$$\mathrm{amp}(V_2) \approx \frac{V_c}{\sqrt{n}}\frac{2\sqrt{\epsilon}}{\sqrt{3\sqrt{ad - bc}(\epsilon\sqrt{ad - bc} - (a + d))}} \tag{46}$$

where n is the Taylor series cubic term of $H(y)$. The equation earlier reveals that the oscillation amplitude with respect to $V_c/\sqrt{n}$ is solely determined by ϵ and the topological parameters a, b, c, and d. It does not depend on the specific OTA, as long as the dominant nonlinearity is cubic, nor whether it is biased above or below threshold. However, the specific values of V_c and ϵ may change with OTA bias region and with OTA topology. Similar observations can be made for OTAs whose nonlinear function $H(y)$ is not dominantly cubic.

C. Inputs to the Nonlinear OTA

We have shown that the input to the nonlinear OTA must be $cx_1 + dx_2$. Fig. 7 shows a generic circuit for generating the inputs in question. Notice that, in the circuit diagram, the argument to the nonlinear OTA is $v_3 = x_1 + x_2 d/c$, instead of $v_2 = cx_1 + dx_2$. Defining $v_3 = v_2/c$, (27) becomes

$$\ddot{v}_3 - (a + d + cg_h H'(cv_3))\,\dot{v}_3 + (ad - bc)\,v_3 = 0. \tag{47}$$

It is then straightfoward to show that the circuit of Fig. 7 meets all of our conditions for oscillator design and that all of our previous results still hold, with the slight correction $\mathrm{amp}(v_3) = \mathrm{amp}(v_2)/c$.

VII. Illustrative Example

In this section, we will apply our oscillator-synthesis procedure to the Lyon/Mead SOS [8] shown in Fig. 8. The oscillator

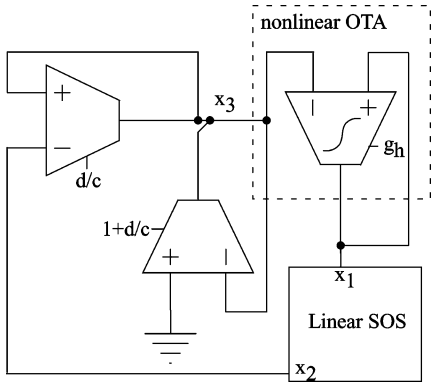

Fig. 7. Inputs to the nonlinear OTA.

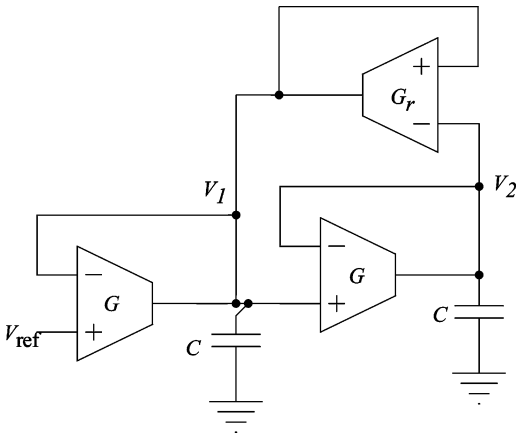

Fig. 8. SOS introduced by Lyon and Mead [8] is normally operated as a low-pass filter. We can apply our synthesis methodology to convert it into an autonomous oscillator with independently controllable amplitude and frequency of oscillation.

designer's choice of SOS topology should normally depend on such considerations as noise and distortion, as addressed by Koziel *et al.*[15]. We chose this particular SOS structure less for any technical merits of the resulting oscillator than for the sheer arbitrariness of it. Our major claim in this paper is that *any* stable SOS can be converted into a controllable well-behaved sinusoidal oscillator. It would not be useful to support this claim with, for example, the circuit of Fig. 6, since it is a lossy resonator, whose conversion to a stable oscillator might seem intuitive almost to the point of being trivial. The Lyon/Mead SOS, however, has traditionally been viewed not as a sinusoidal oscillator but for decades as a simple filter model of the cochlea by the neuromorphic community. Hence, it is probably unlikely to be a contrived demonstration of our synthesis procedure.

A. Placement of the Nonlinear OTA

Applying KCL to nodes V_1 and V_2 of Fig. 8, we get the following set of differential equations:

$$C\begin{bmatrix}\dot{V}_1\\ \dot{V}_2\end{bmatrix}=\begin{bmatrix}G_r-G & -G_r\\ G & -G\end{bmatrix}\begin{bmatrix}V_1\\ V_2\end{bmatrix} \tag{48}$$

where the node voltages are all referenced to V_{ref} and each OTA is assumed to be linear. We make the following definitions:

$$x_1=\frac{V_1}{V_c}\quad x_2=\frac{V_2}{V_c}$$
$$\tau=\frac{t\cdot G}{C}\quad r=\frac{G_r}{G} \tag{49}$$

to get the following dimensionless state-space expression:

$$\begin{bmatrix}\dot{x}_1\\ \dot{x}_2\end{bmatrix}=\underbrace{\begin{bmatrix}r-1 & -r\\ 1 & -1\end{bmatrix}}_{\boldsymbol{A}}\begin{bmatrix}x_1\\ x_2\end{bmatrix}. \tag{50}$$

The transconductance matrix $\boldsymbol{A}$ is Hurwitz for $r<2$, meaning that OTA nonlinearity can convert the SOS shown in Fig. 8 into an oscillator. From our synthesis procedure, we determine that the nonlinear OTA should have a differential input of x_1-x_2, with its output current sourced onto node x_1. From (35) and (50), the small-signal gain of the nonlinear OTA should be

$$g=2+\epsilon-r \tag{51}$$

which, in dimensionalized form, is

$$G_h=(2+\epsilon)G-G_r. \tag{52}$$

When the nonlinear OTA is added to the original Lyon/Mead SOS, we obtain the circuit shown in Fig. 9(a). It should start to oscillate once G_h is larger than $2G-G_r$.

B. OTA Consolidation

Notice from Fig. 9(a) that the nonlinear OTA shares its inputs and output with the G_r OTA. The linear term of the nonlinear OTA renders OTA G_r redundant. We can eliminate this OTA, which implies that $G_r=r=0$. The small-signal gain of the nonlinear OTA is now

$$G_h=(2+\epsilon)G. \tag{53}$$

Fig. 9(b) shows the consolidated circuit, which comprises two linear OTAs and a nonlinear one.

C. Circuit Implementation

The linear OTAs shown in Fig. 9(b) were each implemented as the variable gain OTA of Fig. 10, originally introduced by DeWeerth *et al.*[16]. The attenuation stage is highlighted with a dashed box, where the input voltage is attenuated by the ratio of the transconductance gains of the nMOS differential pair to that of their diode-connected pMOS loads. The nMOS differential pair operates in strong inversion, while the pMOS loads are sized to operate in subthreshold. This gives an attenuation factor of [16]

$$\alpha=\frac{U_T}{\kappa}\sqrt{\frac{2\beta_\alpha}{I_\alpha}} \tag{54}$$

where β_α is a constant that depends on the physical dimensions of the nMOS transistors in the attenuation stage and $I_\alpha\approx 5\ \mu$A is the bias current through this stage.

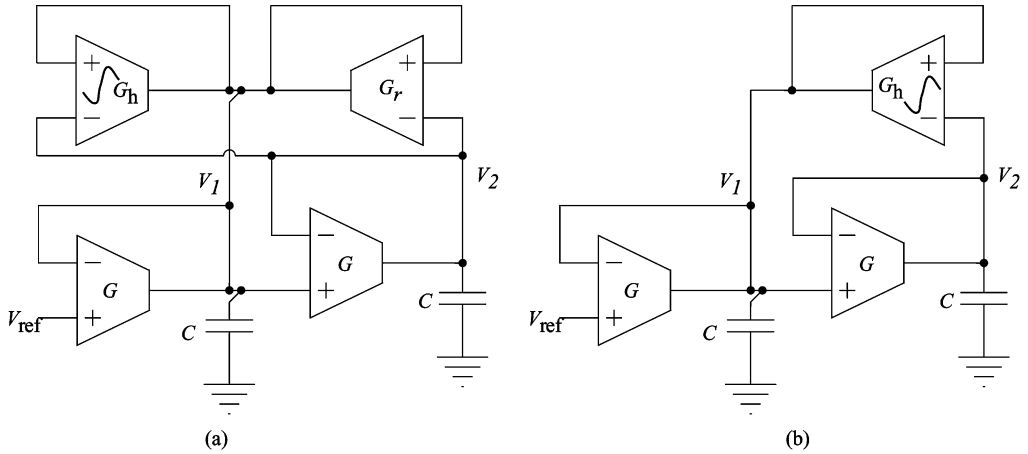

Fig. 9. SOS conversion to an oscillator. (a) OTA-C circuit that results from direct application of synthesis methodology. (b) OTA-C circuit after consolidation. The G_h and G_r OTAs are merged into one, since they share the same input and output nodes.

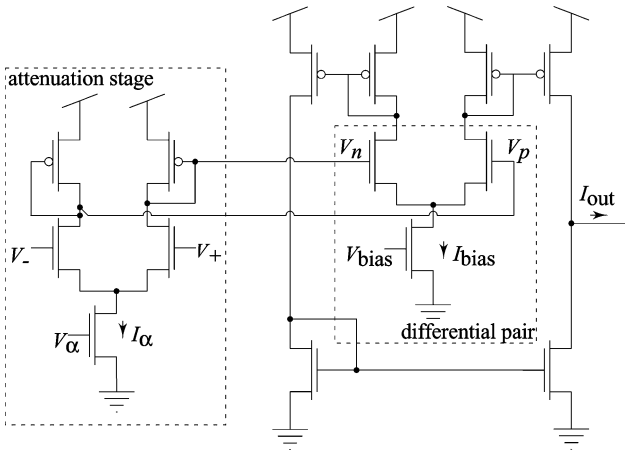

Fig. 10. Variable linear-range OTA. The attenuation stage of the OTA consists of an above-threshold differential pair that is loaded by subthreshold diode-connected transistors. The disparate gains of the above and subthreshold transistors result in voltage attenuation between V_+, V_- and V_p, V_n. The level of attenuation is controlled by the bias current I_α. The output of the attenuation stage is fed to a simple nine-transistor OTA. Transistor dimensions, attenuation stage: nMOS $W/L = 3\mu\text{m}/100\,\mu\text{m}$; pMOS $W/L = 100\,\mu\text{m}/3\,\mu\text{m}$. Current mirror OTA: nMOS $W/L = 20\,\mu\text{m}/3\,\mu\text{m}$; pMOS $W/L = 40\,\mu\text{m}/3\,\mu\text{m}$.

The nonlinear OTA was implemented as a current-mirror nine-transistor OTA, i.e., the circuit shown in Fig. 10, minus the attenuation stage. The attenuation factor for the nonlinear OTA is effectively fixed at $\alpha = 1$.

The on-chip capacitors were fabricated as poly–polycapacitors with $C = 912.5$ fF. The parasitic input capacitance of the attenuators (on the order of 1 pF) add to these poly–polycapacitors, making the total effective capacitance hard to predict precisely. A correction term must therefore be factored into the frequency-of-oscillation equation.

D. Experimental Results

We fabricated the OTA-C circuit shown in Fig. 9(b) in a 0.5-μm process available from MOSIS. The die photo is shown in Fig. 11. We had control of the bias currents through the bias transistors' gate voltages. The nodes V_1 and V_2 were accessible via on-chip buffers. The OTAs ran on a single-ended supply of 3.3 V and had a bandwidth of a few hundred kilohertz.

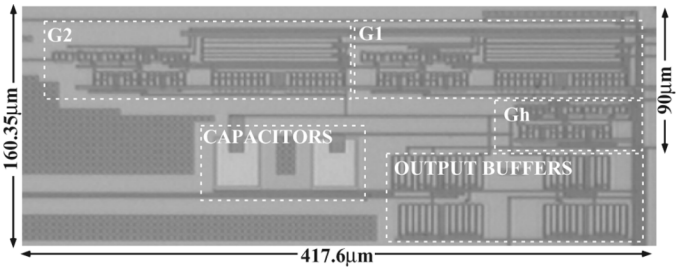

Fig. 11. Oscillator die micrograph. The labeled portions correspond to the circuit components in Fig. 9(b). Total area, including output buffers, is 160.35 μm$\times$ 417.60 μm.

For subthreshold operation, the transconductance gains were defined as

$$G = I_{\text{avg}} \cdot \frac{\alpha\kappa}{2U_T} \tag{55}$$

$$G_h = \underbrace{\alpha I_{\text{avg}}(2+\epsilon)}_{I_h} \cdot \frac{\kappa}{2U_T} \tag{56}$$

where I_{avg} and I_h are the bias currents of the linear and nonlinear OTAs, respectively. According to (40), the frequency of oscillation should be equal to

$$f = \frac{\alpha\kappa I_{\text{avg}}}{4\pi C U_T} \quad \text{(in Hz)}. \tag{57}$$

Fig. 12 is a plot of (57), superimposed on measurement results. Given the uncertainty of the exact value of C, the values $\alpha = 0.1$ and $\kappa = 0.67$ were chosen to fit the data. The figure shows a linear tuning range of 2.2–100 kHz. The prototype OTAs suffered from low bandwidth, relative to oscillating frequency. Thus, to keep amplitude constant across the frequency range, the ratio I_h/I_{avg} was manually varied from 0.44 to 0.37 to offset parasitic effects [3]. The power consumption varies over this tuning range from 0.19 to 6.27 μW. If we opt for above-threshold operation, we can push the frequency of oscillation into the low 200-kHz range.

Equation (42) predicts that the amplitude of oscillation is $V_{\text{amp}} = 4\text{m}_{gh}\text{V}_c\text{V}_{pp}$. We defined m_{gh} as the solution to $H'(m_{gh}) = 2/(g_h)$. For our nonlinear OTAs operated in the

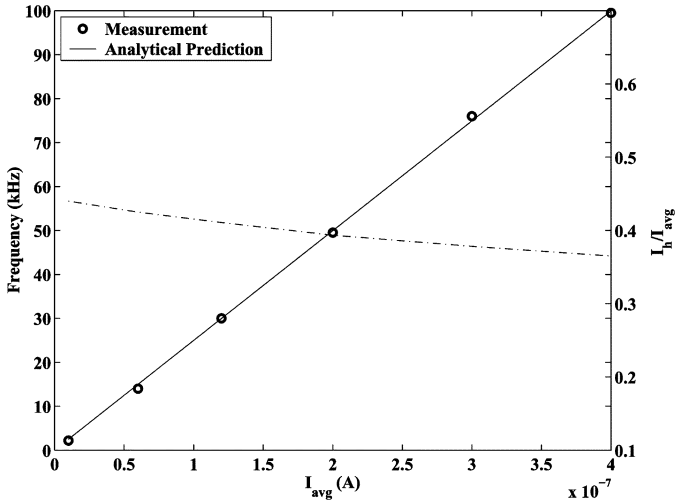

Fig. 12. Linear frequency control with current $I_{\rm avg}$, at 100-mV_{pp} oscillation amplitude. Increasing the current increases each transconductance gain G proportionally, causing a linear increase in the oscillation frequency. The dashed line (y axis on the right) is a plot of the ratio of $I_h/I_{\rm avg}$ across this range of frequencies. Ideally, this ratio should be fixed for a constant amplitude of oscillation. However, we manually changed the ratio across frequencies to offset parasitic capacitances in the OTAs.

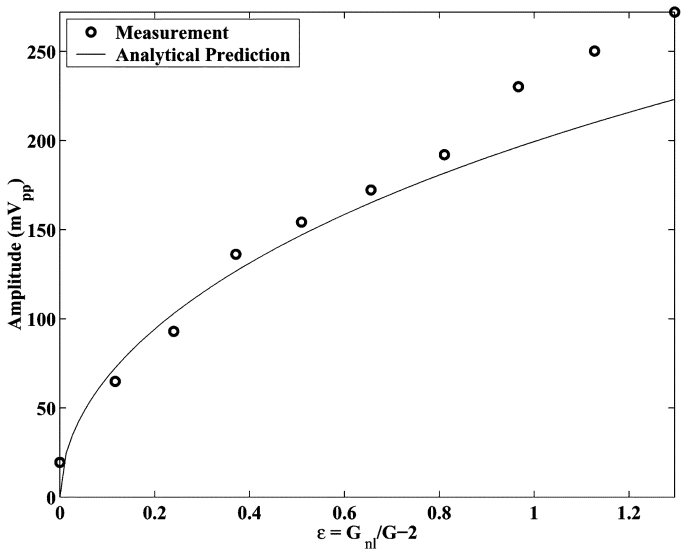

Fig. 13. Amplitude control with transconductance G_h, at 100-kHz oscillation frequency. The transconductance G_h is directly proportional to ϵ. From (59), the amplitude of oscillation is roughly proportional to $\sqrt{\epsilon}$.

subthreshold region, $H(\cdot) = \tanh(\cdot)$. Hence, m_{gh} is found to be

$$m_{gh} = \tanh^{-1}\left(\sqrt{(g_h-2)/(g_h)}\right) = \tanh^{-1}\left(\sqrt{\frac{\epsilon}{\epsilon+2}}\right) \quad (58)$$

and the (subthreshold) amplitude of oscillation is

$$V_{\rm amp} = 8\frac{U_T}{\kappa}\tanh^{-1}\left(\sqrt{\frac{\epsilon}{\epsilon+2}}\right)(V_{pp}). \quad (59)$$

We took experimental measurements of oscillation amplitude versus ϵ and compared our results to the analytical expression of (59). Fig. 13 shows this comparison.

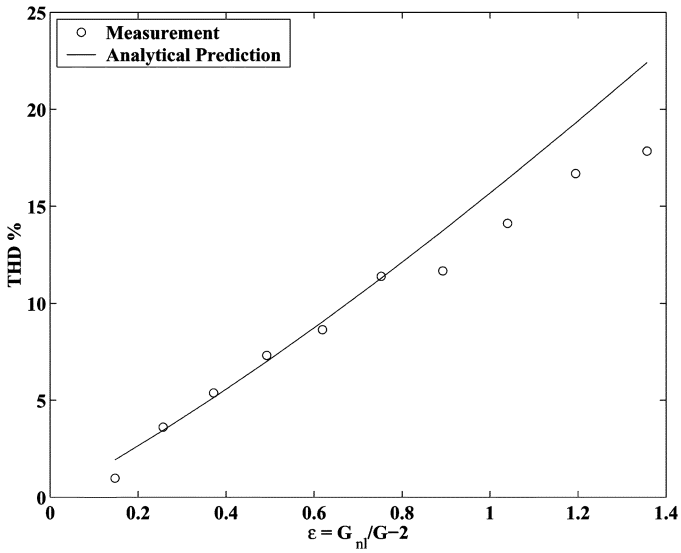

Fig. 14. THD exhibits a linear dependence on transconductance gain G_h, as predicted by (39). These THD measurements are for an oscillation frequency of 20 kHz and include harmonics up to the tenth.

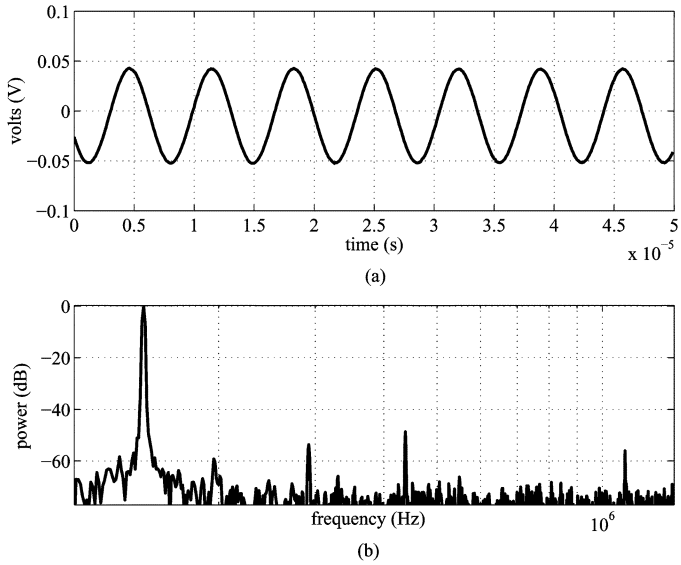

Fig. 15. Oscillator output for 90 mV_{pp} at 146 kHz. (a) Timeseries. (b) Power spectrum. The even-order harmonics are due to input offset in the linear OTAs. THD calculated up to the tenth harmonic is 0.47%. Phase noise is -66 dBc/Hz at a 10-kHz offset.

We showed in Section V that the oscillator's THD depends on ϵ as

$$THD\% \approx 12.5\epsilon + 3.8\epsilon^2.$$

Experimental results (see Fig. 14) show a similar trend to that given by the THD equation. Comparing Figs. 13 and 14, observe that the analytical predictions based on the van der Pol model begin to diverge from measured data as ϵ becomes too large for the synthesized nonlinear resistor to be validly approximated as a simple cubic. In addition, fairly high amounts of THD are experienced for relatively small oscillation amplitudes. We can achieve higher oscillation amplitudes with less THD if we operate the OTAs above threshold.

Fig. 15 shows a typical measured output power spectrum for when the oscillator is operated above threshold. Here, $I_{\rm avg} =$

10 μA and $\epsilon \approx 0.03$. The resulting oscillation is at 146 kHz with a 90-mV_{pp} amplitude and a THD of only 0.47% (compare this to the subthreshold case, where an oscillation amplitude of 90 mV would cause a THD of approximately 3%).

The unexpected feature of Fig. 15 is that the power spectrum reveals a second harmonic, despite our theoretical solution (38), having no even-order harmonics. The second harmonic is caused by input offset in the OTA differential pair. Input offset refers to the nonzero differential input voltage at which an OTA has an output current of 0 A. Consider the differential pair of Fig. 10 and say it has an offset of V_{off}. Then the output current of the OTA can be written as

$$I_{\text{out}} = F(V_p - V_n - V_{\text{off}}) \tag{60}$$

where $F(\cdot)$ is some function such that $F(0) = 0$ and V_p and V_n are the differential-pair input voltages. In terms of the *OTA inputs*, V_+ and V_-, we write (60) as

$$\begin{aligned} I_{\text{out}} &= F(\alpha(V_+ - V_-) - V_{\text{off}}) \\ &= F\left(\alpha\left(V_+ - V_- - \frac{V_{\text{off}}}{\alpha}\right)\right) \end{aligned} \tag{61}$$

which shows that the intrinsic offset of the differential pair has been magnified by $1/\alpha$. The effect of this magnification is so detrimental that the second harmonic has a magnitude of -55 dBc. Because our distortion analysis ignored this effect, our THD equation is not all that accurate. Still, our experimental results shown in Fig. 14 are reasonably close to our predicted values.

The power spectrum of an ideal sinusoid should have a delta function at its oscillation frequency. As Fig. 15 shows, a physically derived sinusoid displays some spreading in the power spectrum, resulting in "skirts" around the oscillation frequency. This nonideality is normally quantified as phase noise [17]. For the operating point shown in Fig. 15, the phase noise is -66 dBc/Hz at a 10-kHz offset. Earlier work has provided analytical expressions for the expected phase noise of a van der Pol oscillator [18].

VIII. Discussion

Although we focused on input attenuation as a form of OTA linearization, there are many other schemes that deign to linearize an OTA without an explicit attenuation stage [6], [20]. As we previously showed, one reason to do this is to avoid the input offset amplification that an attenuation stage creates. Thus, linear OTAs used in actual oscillators might very well not have attenuation stages at all. This fact does not make our results any less valid; all that our analyses assume is the availability of linear OTAs and of one sigmoidally nonlinear OTA.

For a van der Pol oscillator, the oscillation amplitude with respect to the characteristic voltage V_c is uniquely determined by ϵ, the specific implementation of $H(y)$, and the relationships among the SOS topological parameters a, b, c, and d. On the other hand, THD depends only on ϵ and not on V_c or on the SOS topology. Consequently, the only way to increase amplitude while keeping THD (i.e., ϵ) constant is to find a better SOS topology, to increase the value of V_c, or to change the implementation of $H(y)$. As the SOS topology may have been optimized according to some other criterion such as low noise, we will assume that it is fixed. Therefore, the two options left for increasing oscillation amplitude are to increase V_c (for our example OTAs, this can be done by increasing the bias current when in above threshold) or to change the analytical form of $H(y)$ using, for example, bump linearization [20].

The sigmoidal function $H(y)$ of a perfectly bump-linearized OTA is not cubic but is rather a dominantly fifth-order nonlinearity. An oscillator built with such an OTA, or any other OTA with a noncubic-dominant nonlinearity, would not be a van der Pol oscillator. However, it would still fall under the general description of (13), and the methods for its analysis are identical to that of the van der Pol oscillator.

IX. Conclusion

In this paper, we have presented a framework for exploiting OTA nonlinearity in the design of OTA-C oscillators. Our method is based on an examination of the OTA transfer function and on insight into the kind of dynamics that such a transfer function would yield. The rigor of our method allows us to do a theoretical analysis of the oscillator's performance. We have demonstrated our oscillator synthesis procedure with a simple three-OTA circuit. The experimental results from this oscillator circuit support the predictions that our analysis makes.

References

[1] A. Buonomo, C. Di Bello, and O. Greco, "A criterion of existence and uniqueness of the stable limit cycle in second-order oscillators," *IEEE Trans. Circuits Syst.*, vol. CAS-30, no. 9, pp. 680–683, Sep. 1983.

[2] A. Buonomo, C. Di Bello, and A. L. Shiavo, "On the analysis and design of second-order harmonic oscillators," in *Proc. ISCAS*, May 2000, vol. 1, pp. 623–626.

[3] A. Rodriguez-Vazquez, B. Linares-Barranco, J. L. Huertas, and E. Sanchez-Sinencio, "On the design of voltage-controlled sinusoidal oscillators using OTAs," *IEEE Trans. Circuits Syst.*, vol. 37, no. 2, pp. 198–211, Feb. 1990.

[4] B. Linares-Barranco, T. Serrano-Gotarredona, J. Ramos-Martos, J. Ceballos-Cáceres, J. M. Mora, and A. Linares-Barranco, "A precise 90° quadrature OTA-C oscillator tunable in the 50–130-MHz range," *IEEE Trans. Circuits Syst. I, Reg. Papers*, vol. 51, no. 4, pp. 649–663, Apr. 2004.

[5] J. A. De Lima and P. R. Agostinho, "A low-voltage low sensitivity sinusoidal VCO for DPLL realizations," in *Proc. ISCAS*, May 2004, pp. 789–792.

[6] J. Galan, R. G. Carvajal, A. Torralba, F. Munoz, and J. Ramirez-Angulo, "A low-power low-voltage OTA-c sinusoidal oscillator with a large tuning range," *IEEE Trans. Circuits Syst. I, Reg. Papers*, vol. 52, no. 2, pp. 283–291, Feb. 2005.

[7] T. Serrano-Gotarredona and B. Linares-Barranco, "7-decade tuning range cmos OTA-c sinusoidal VCO," *Electron. Lett.*, vol. 34, no. 17, pp. 1621–1622, Aug. 1998.

[8] R. F. Lyon and C. Mead, "An analog electronic cochlea," *IEEE Trans. Acoust., Speech Signal Process.*, vol. 36, no. 7, pp. 1119–1134, Jul. 1988.

[9] C. C. Enz, F. Krummenacher, and E. A. Vittoz, "An analytical mos transistor model valid in all regions of operation and dedicated to low-voltage and low-current applications," *Analog Integr. Circuits Signal Process.*, vol. 8, no. 1, pp. 83–114, Jul. 1995.

[10] P. E. Allen and D. R. Holberg, *CMOS Analog Circuit Design*. New York: Oxford Univ. Press, 2002.

[11] L. Perko, *Differential Equations and Dynamical Systems*. New York: Springer-Verlag, 2001.

[12] B. Van der Pol, "On relaxation oscillations," *Philos. Mag.*, vol. 27, pp. 978–992, 1926.

[13] B. Linares-Barranco, A. Rodriguez-Vazquez, E. Sanchez-Sinencio, and J. L. Huertas, "Generation, design and tuning of OTA-C high frequency sinusoidal oscillators," *Proc. Inst. Elect. Eng.—Circuits Devices Syst.*, vol. 139, no. 5, pp. 557–568, Oct. 1992.

[14] R. Rand, *Lecture Notes on Nonlinear Vibrations*. Ithaca, NY: Internet-First Univ. Press, 2003.

[15] S. Koziel, R. Schaumann, and H. Xiao, "Analysis and optimization of noise in continuous-time OTA-C filters," *IEEE Trans. Circuits Syst. I, Reg. Papers*, vol. 52, no. 6, pp. 1086–1094, Jun. 2005.
[16] S. P. DeWeerth, G. N. Patel, and M. F. Simoni, "Variable linear-range subthreshold OTA," *Electron. Lett.*, vol. 33, no. 15, pp. 1309–1311, Jul. 1997.
[17] B. Razavi, *RF Microelectronics*. Upper Saddle River, NJ: Prentice-Hall, 1998.
[18] B. N. Limketkai and R. W. Brodersen, "An equation-based method for phase noise analysis," in *Proc. CICC*, Sep. 2003, pp. 703–706.
[19] V. Srinivasan, G. J. Serrano, J. Gray, and P. Hasler, "A precision CMOS amplifier using floating-gates for offset cancellation," in *Proc. CICC*, Sep. 2005, pp. 734–737.
[20] R. Sarpeshkar, R. F. Lyon, and C. Mead, "A low-power wide-linear-range transconductance amplifier," *Analog Integr. Circuits Signal Process.*, vol. 13, no. 1–2, pp. 123–151, May 1997.

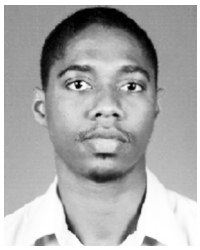

Kofi M. Odame (S'06) received the B.Sc. and M.Sc. degrees in electrical and computer engineering from Cornell University, Ithaca, NY, in 2002 and 2004, respectively. He is currently working toward the Ph.D. degree in the School of Electrical and Computer Engineering, Georgia Institute of Technology, Atlanta.

His research interest includes harnessing the inherent nonlinear characteristics of circuit devices to design cheap and efficient continuous-time processing systems.

Paul Hasler (SM'02) received the B.S.E. and M.S. degrees in electrical engineering from Arizona State University, Tempe, in 1991 and the Ph.D. degree in computation and neural systems from California Institute of Technology, Pasadena, in 1997.

He is currently an Associate Professor with the School of Electrical and Computer Engineering, Georgia Institute of Technology, Atlanta. His current research interests include low-power electronics, the use of floating-gate MOS transistors to build adaptive information processing systems, and "smart" interfaces for sensors.

Dr. Hasler was the recipient of the National Science Foundation CAREER Award in 2001, and the Office of Naval Research YIP Award in 2002. He was also the recipient of the Paul Raphorst Best Paper Award from the IEEE Electron Devices Society in 1997, a Best Student Paper at CICC 2005, a Best Sensors Track Paper at ISCAS 2005, a Best Paper Award at SCI 2001, and a Finalist for the Packard Young Investigator Award in 1999.